Design Under Uncertainty for Conceptual Aircraft Design Leveraging Analytical Gradients

Ben D. Phillips* and Joanna N. Schmidt†
NASA Langley Research Center, Hampton, VA, 23681

Eliot D. Aretskin-Hariton ‡ and Robert D. Falck §
NASA Glenn Research Center, Cleveland, OH, 44135

The purpose of this paper is to extend previously demonstrated methodologies for design under uncertainty, leveraging analytical gradients to higher fidelity analysis for use in conceptual aircraft design. Previous work developed methods to generate analytical derivatives through polynomial chaos expansion, eliminating the need to estimate derivatives via complex step or finite difference. In this research, the authors build upon the methods to include physics-based aircraft design codes for aircraft design under uncertainty. This extends the previous work's case study, which employed analytical aerodynamics and Breguet range estimations for wing design, to a higher fidelity level. In addition, this work extends previous work on interface development between the Uncertainty Quantification with Polynomial Chaos Expansion (UQPCE) software and Model-Based Systems Analysis and Engineering (MBSA&E) frameworks. This paper will discuss the development work necessary to perform multidisciplinary design under uncertainty as well as demonstrate the mechanics of interfacing UQPCE and conceptual aircraft design tools such as NASA's Aviary code. In a case study, a conceptual aircraft design under uncertainty was conducted and compared against a traditional deterministic design. When given information about the uncertainty space from UQPCE, the optimizer was able to shape the output distribution and produce a more robust design.

Nomenclature

A_i	Undetermined PCE Coefficients	P	Number of Terms in PCE Model
a	Significance Level	P_{minx}	Chordwise Location of Minimum Pressure
b	Span	p	Order of PCE Model
d	PCE Deterministic Variables	$\mathcal{R}_z$	Residual of Implicit Output, z
F	PCE Response	$\vec{x}$	Vector of Resampled PCE Values
$\bar{f}$	Activation Function	$\boldsymbol{\xi}$	PCE Random Variables
M	Mach Number	z	PCE Confidence Interval Bound
N_t	Number of Terms Necessary for PCE Model	Λ	Wing Leading Edge Sweep Angle
n	Number of Uncertain Parameters in PCE Model	μ	Mean
n_{an}	Function Calls for Analytical Derivatives	Ψ_i	PCE Basis Functions i^{th} Mode
n_{dv}	Function Optimization Design Variables	σ	Standard Deviation
n_{fd}	Function Calls for Finite Difference	ω	Activation Function Tuning Parameter
n_{pce}	Function Calls for PCE at Each Step		

I. Introduction

To realize the aggressive goals of the U.S. Aviation Climate Action plan and achieve net-zero greenhouse gas emissions of aircraft by 2050 [1], unconventional aircraft and new technologies will likely need to be deployed fleet-wide. There are a significant number of uncertainties associated with new aircraft types and yet-to-be-developed technologies.

*Aerospace Engineer, Aeronautics Systems Analysis Branch, Systems Analysis and Concepts Directorate.
†Aerospace Engineer, Aeronautics Systems Analysis Branch, Systems Analysis and Concepts Directorate.
‡Aerospace Engineer, Propulsion Systems Analysis Branch
§Aerospace Engineer, Mission Architecture and Design Branch. Member AIAA

Particularly challenging is the inclusion of these uncertainties in the conceptual design phase. Historically, aircraft conceptual design leverages regression-based models, which have been calibrated to similar previously designed, manufactured, and operated. When developing an "unconventional"concept such as a blended wing body or hydrogen powered aircraft, historical data to inform the regression-based models does not exist. A further complicating factor in incorporating these uncertainties is the highly coupled nature of proposed technologies such as distributed electric propulsion (DEP), boundary layer ingestion (BLI), truss-braced wings (such as those on the X-66), and general electrified aircraft propulsion (EAP). To better understand the potential impact of new aircraft and technologies, the above uncertainties must be considered in the design process.

When performing system-level optimization under uncertainty, each individual discipline usually presents its own specific uncertainties. These discipline-specific uncertainties and their interactions have to be included when modeling a system-level metric such as aircraft fuel burn. Figure 1 shows a general depiction of the discipline-level uncertainties and the overall system-level uncertainties. First, the tools and methods must be capable of performing the analysis to assess the vehicle-level uncertainties. Once the capability exists to predict the probabilistic output of interest, a design framework can leverage that information to mitigate the potential negative impact of uncertainties.

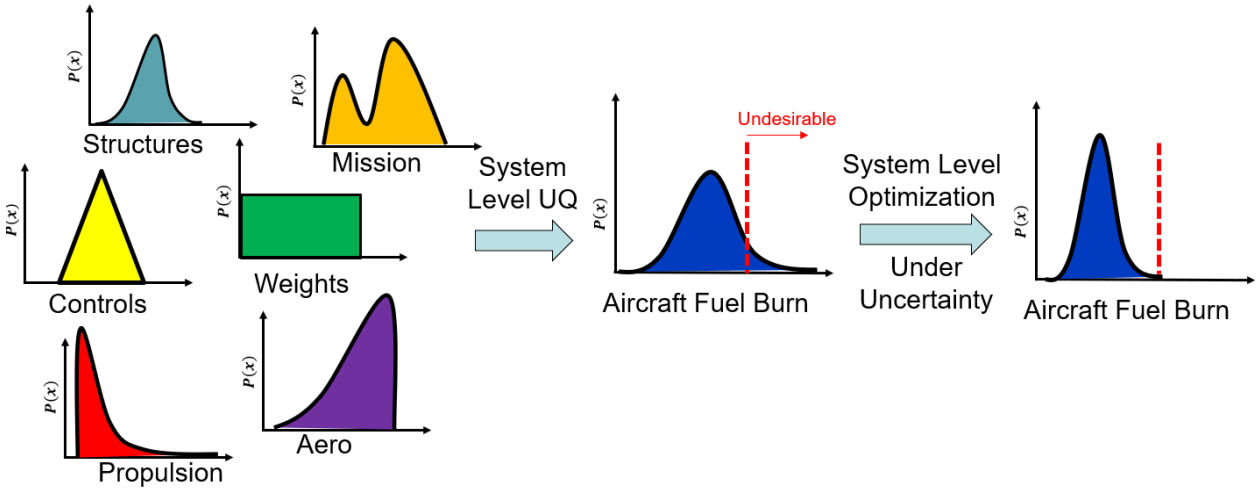

Fig. 1 Infographic of design under uncertainty at the system level.

Uncertainty quantification (UQ) has been typically used in conceptual aircraft design as a post-optimality assessment after an optimization or analysis is completed. In contrast, this paper explores the implications of performing UQ as an integrated part of an optimization, allowing statistical-based metrics to formulate objectives and constraints for the optimizer. The methodology (section II) contains details on the implementation of Uncertainty Quantification with Polynomial Chaos Expansion (UQPCE) for use with gradient-based optimization and builds upon previous work presented by Phillips et al. [2]. Following that, a case study (Section III) is presented which applies the UQPCE implementation to the N3CC aircraft model. The N3CC is a NASA-developed 154-passenger aircraft [3, 4] shown in Fig. 2. Results and discussion on the methods are then presented in Section III.E, with final conclusions given in Section IV.

II. Methodology

This section is divided into two subsections: the first section introduces UQPCE and the second section introduces the approach to obtain analytical derivatives for the confidence interval generated from a polynomial chaos model. Generally speaking, UQ encompasses the study of the impact of uncertainties in input parameters and modeling simplifications on the outputs or responses of a process or simulation. UQ can vary in scope by including only a single model or multiple models of varying fidelity levels as well as experimental data. The overarching objective of UQ is to create a more robust design or evaluation process by identifying sensitivities and mitigating the potential impact of uncertainties through informed, targeted resource investments. Two main types of uncertainty are present in most simulations: model input uncertainty and model form uncertainty. Model input uncertainty refers to uncertain sources feeding the model such as initial conditions, boundary conditions, or input parameters. Model form uncertainty refers to limitations in the methods or applications themselves such as simplifying assumptions or missing physics. An important

Fig. 2 N3CC base model.

facet of UQ is the proper characterization and treatment of the model input uncertainties [5, 6]. Some of the techniques utilized in this work include second-order probability analysis and point collocation non-intrusive polynomial chaos. The reader is referred to previous work by Phillips and West [7] and Eldred [8] for more details.

A. Uncertainty Quantification with Polynomial Chaos Expansion (UQPCE)

All of the uncertainty modeling and analysis contained in this research was performed with one of NASA's in-house uncertainty codes: UQPCE [9]. UQPCE* is an open source, Python-based research code for use in parametric, non-deterministic computational analysis and design. UQPCE utilizes a non-intrusive polynomial chaos expansion surrogate modeling technique to efficiently estimate uncertainties for computational analyses. The software enables the user to perform an automated uncertainty analysis for any given computational code without requiring modification to the source. UQPCE estimates sensitivities, confidence intervals, and other model statistics which can be useful in the conceptual design and analysis of flight vehicles. This software was originally developed with funding from the Commercial Supersonic Technology (CST) Project to study the potential impacts of uncertainties on the prediction of ground noise generated from commercial supersonic aircraft concepts [7, 10–13]. The code development is currently supported by the Transformational Tools and Technologies (TTT) project and has been leveraged in uncertainty analysis for electrified aircraft propulsion studies [14], integration with Model-Based Systems Analysis and Engineering (MBSA&E) [15], and other internal unpublished systems analysis work.

B. Analytical Derivatives for PCE-Generated Confidence Intervals

To leverage the full capability of polynomial chaos expansion (PCE) for design under uncertainty, integration with a gradient-based optimization framework such as OpenMDAO [16] is necessary. OpenMDAO is an open source Python framework for multidisciplinary design analysis and optimization. The modular analysis and unified derivatives (MAUD) framework implemented in OpenMDAO for calculating total derivatives only requires each component to provide partial derivatives. If partial derivatives for uncertain components can be provided in an analytical format to OpenMDAO, a gradient-based optimization can perform without any further development or modifications to the optimizer itself.

Implementing a PCE approach in a gradient-based design under uncertainty problem requires a PCE model be assembled at each point within the design space (i.e., each step the optimizer takes). However, each PCE model only gives estimates for statistical parameters (e.g., mean, variance, confidence intervals, sensitivities, etc.) at that step. As noted in Ref. [8], the PCE models at each step are only valid for those particular values of the design variables and must be recalculated when the design variables are changed. To estimate derivatives at each step with a method such as finite difference, multiple PCE models are necessary. The computational cost of these models scales with the order of the PCE expansion, the number of uncertain parameters, and the number of design variables. For any moderately expensive underlying analysis, this process quickly becomes computationally intractable for cases with more

*https://github.com/nasa/UQPCE

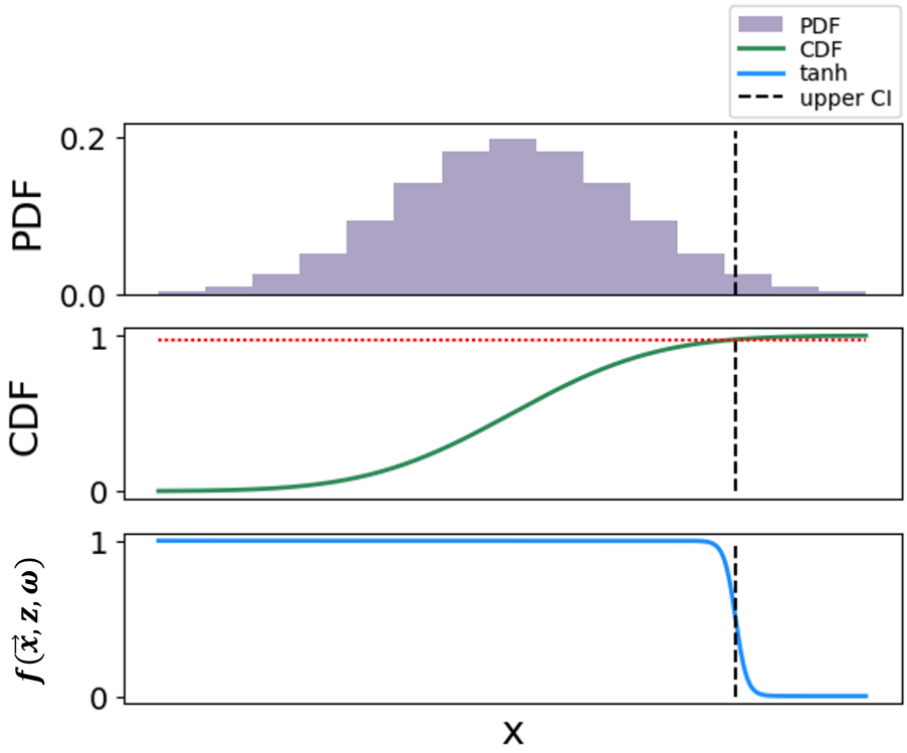

Fig. 3 Example Probability Density Function (PDF), Cumulative Distribution Function (CDF), and activation function of a normal distribution.

than tens of design or uncertain parameters. Furthermore, when mixed uncertainty problems are being considered, a confidence-interval-informed objective function is required, which also adds non-negligible computational costs. Finite difference or complex step approximations of derivatives are often not computationally efficient options for incorporating uncertainty as constraints or objectives in an optimization.

Obtaining analytical derivatives of points on a confidence interval through a traditional process would involve differentiation through a binning procedure. Instead of attempting to model the binning, the prior work [2] used an implicit function theorem and a smooth counting function to generate an approximation that is sufficiently accurate when the number of data points involved is sufficiently large. Equation (1) is effectively a continuous counting function that provides an approximate count of the number of elements in $\vec{x}$ that are less than or equal to z.

$$\bar{f}(\vec{x}, z, \omega) = 1 - \frac{(1 + \tanh(\frac{\vec{x}-z}{\omega}))}{2} \tag{1}$$

The parameter ω determines how abrupt the transition from 0 to 1 is in the vicinity near z. As ω approaches zero, the response more accurately models a step function, whereas larger values provide a smoother derivative. Figure 3 shows the Probability Density Function (PDF), Cumulative Distribution Function (CDF), and associated activation function for a normal distribution. The vertical dashed lines in the figure represent the chosen significance level for the confidence interval and the corresponding location on the PDF, CDF, and activation function.

For a selected significance level a equal to 0.05, 95% of the data fall within the confidence interval, with 2.5% falling above the upper end of the interval. The residual equation that governs the value of the 95% confidence interval, z, is thus:

$$\mathcal{R}_z(\vec{x}, z, \omega) = \sum_{i=1}^{n} \bar{f}_i(\vec{x}, z, \omega) - 0.975n \tag{2}$$

The partial derivatives for the residual with respect to both $\vec{x}$ and z are needed. Although these derivatives can be approximated using finite difference or complex step, it is not uncommon for $\vec{x}$ to have a length on the order of millions; approximating the derivatives quickly becomes expensive. The analytical derivatives below are provided to OpenMDAO to avoid unnecessary computational expense.

$$\frac{\partial \mathcal{R}_z(\vec{x}, z, \omega)}{\partial x} = \frac{-1}{2\omega \cosh^2(\frac{\vec{x}-z}{\omega})} \tag{3}$$

$$\frac{\partial \mathcal{R}_z(\vec{x}, z, \omega)}{\partial z} = \sum_{i=1}^{m} \frac{1}{2\omega \cosh^2(\frac{\vec{x}-z}{\omega})} \tag{4}$$

Note that although the above implementation of analytical derivatives was used for the analysis in this case study, OpenMDAO now has the activation function implemented natively using the software package JAX [17] to calculate the derivatives. Equation 2 is differentiable with respect to z and can be efficiently solved using a Newton solver. To utilize z as an objective or constraint in gradient-based optimization, its total derivative with respect to the data $\vec{x}$ needs to be computed. OpenMDAO is used to eliminate the residual using a Newton solver and then efficiently compute derivatives of z with respect to the data $\vec{x}$ by applying the implicit function theorem to Eq. (2). Since $\mathcal{R}_z$ is a scalar value, this derivative can be evaluated with a single linear solve in reverse mode as opposed to n linear solves in forward mode. The hyperbolic tangent activation function can be susceptible to issues due to vanishing gradients when elements of $\vec{x}$ are far from z, but the authors' experience using the mean and variance estimation output from the PCE model to inform the value of z_{guess} has lessened this concern. It is possible that more a priori information about the uncertainty space may be required if the location of the 95% confidence interval is significantly far away from the variance-informed value of z_{guess} shown in Eq. (5).

$$z_{guess} = \mu + 2\sigma \tag{5}$$

When epistemic uncertainties are present in a system, the bound on uncertainty is determined by finding the confidence interval from the outer lower and upper curves. Two steps are followed to find this bound on uncertainty while preserving the analytical derivatives throughout the calculation. First, the confidence interval of each individual curve is calculated following the above hyperbolic tangent method; this preserves the differentiability of the solved confidence interval values for all curves. Second, the minimum or maximum of these individual confidence intervals is calculated using OpenMDAO's implementation of the Kreisselmeier-Steinhauser (KS) function. This results in a differentiable bound on the uncertainty for a system that includes both aleatory and epistemic uncertainties. This technique coupled with the incorporation of analytical derivatives through an multidisciplinary design optimization (MDO) process eliminates the need to estimate derivatives, which are usually derived from finite difference, complex step, or similar methods. Developing a differentiable confidence interval enables mixed uncertainty problems to be modeled whereas previous methods were unable to represent objective functions containing statistical quantities such as mean and variance.

The cost per iteration of conducting a gradient-based optimization incorporating uncertainty with PCE and finite difference to estimate gradients, n_{fd}, is given by Eq. (6).

$$n_{fd} = n_{pce}(n_{dv} + 1) \tag{6}$$

where n_{pce} is the number of terms necessary to build the PCE model and n_{dv} is the number of design variables in the optimization. Conversely, the cost per iteration of conducting a gradient-based optimization incorporating uncertainty with PCE and analytical gradients to obtain gradients, n_{an}, is given by Eq. (7).

$$n_{an} = n_{pce} \tag{7}$$

From Eqs. (6) and (7), the cost savings of design under uncertainty for gradient-based optimization leveraging analytical gradients through PCE scales with the product of the number of terms necessary to build the PCE model and the

number of design variables, $n_{pce}n_{dv}$. The addition of analytical derivatives to a polynomial-chaos-based UQ method can decrease the computational costs of performing design under uncertainty by orders of magnitude in comparison with methods such as finite difference or complex step. The significant decrease in costs can enable future work in system-level optimization problems requiring high-fidelity analysis.

C. Physics-Based Tools

This section will introduce the physics-based tools used in the demonstration case for this paper, along with detailing improvements to these tools performed to enable this research.

1. Mission Analysis

Aviary [18–20] is NASA's open source conceptual aircraft design tool which leverages gradient-based methods to perform analysis and optimization. Aviary is built on the OpenMDAO library and leverages Dymos [21] to simulate user-designed mission analysis. The software contains aircraft sizing and analysis tools for aerodynamics, weights, structures, propulsion, and mission. Aviary can be coupled with higher fidelity analysis to delve deeper into any of these disciplines or other disciplines such as EAP in coupling with the aircraft design. The heritage of Aviary comes from the General Aviation Synthesis Program (GASP) [22] and the Flight Optimization System (FLOPS) [23]. These tools are currently in use by government and academia but are lacking in their ability to perform coupled optimization as that was not the focus at the time they were designed. In this work, the core Aviary aerodynamics and weights modules are used. To enable design under uncertainty within the Aviary code for this research, two new capabilities were added to core Aviary: a multi-mission optimization capability and an off-design capability.

The multi-mission instantiates multiple Aviary problems as sub-groups inside of a single "super problem."The optimization is monolithic, containing only a single optimizer and no sub-optimization. This enables a single aircraft design to be flown through multiple missions simultaneously. The resulting fuel burn from each mission is then summed and used as the objective. Additionally, the ability to differentiate between the design number of passengers and as-flown number of passengers was also added. This capability enables designers to optimize the vehicle across multiple different mission types (stage lengths, trajectories, atmospheres) as well as add a weighting to each individual mission.

An off-design mission capability was developed which enables previously optimized aircraft to be flown on a new mission, allowing new payload and mission parameters without changing any other design parameters of the aircraft. This enables post-optimality uncertainty quantification by optimizing for a single design mission and then assessing alternative missions.

2. Geometry

An OpenVSP [24] geometry of the N3CC aircraft was used as a base model for this work (see Fig. 2). OpenVSP geometry was leveraged to enable wing area calculations to be updated within the optimization as the geometric design variables are changed. To obtain derivatives across the geometry with respect to area, the finite difference method was employed. An alternative to this approach could be building surrogate models for wing area from OpenVSP prior to the optimization. In this case, the wing area surrogate model, with analytical derivatives, would replace OpenVSP within the optimization. Making this substitution can reduce the computational costs by an order of magnitude. Future work will be dedicated to the incorporation of analytical derivatives for geometric design variables from OpenVSP to decrease computational costs.

III. Case Study

This section will first introduce the problem formulation including the source of the uncertain parameters and their modeling. Then, results from a baseline uncertainty analysis will be detailed. Next, the optimization problem formulation, design variables, and objective functions will be introduced. Finally, results from the optimization problems will be discussed.

A. Problem Formulation

The N3CC aircraft was modeled in the Aviary framework. This model served as the initial configuration for the case study optimization problem. The optimization problem objective, constraints, and uncertain parameters were all derived from theoretical mission requirements of a 3000 nmi segment which must be be completed three times daily. Starting

with a time constraint of 24 hr (1440 min), each leg was given a nominal 60 min for aircraft turnaround. The aircraft turnaround time is the time required to taxi to the gate, unload passengers and cargo from the previous flight, load the passengers, cargo, and fuel for the next flight, and taxi for departure. This required each mission to complete (takeoff to touchdown) in 430 min.

Uncertainty was injected into the time component of the mission via the amount of time required to turn around the aircraft. Limited publicly available data from OAG [25] were used to build a triangular distribution for time necessary aircraft turnaround. Comparing the actual turnaround time for narrow body aircraft from the five largest US airlines in March 2023 to the planned turnaround time formed the basis for the uncertainty distribution. The largest difference in average planned versus actual time was 13 min. As this was an average, the upper bound on the triangular distribution was set as twice as much, or 60 min + 26 min = 86 min. In this case, the mission must complete within 404 min instead of the nominal 430 min to maintain the three daily missions. For ease of solver convergence, the uncertainty in mission time was converted to uncertainty in cruise Mach number. The time constraints translated from [430 min, 404 min] to a cruise Mach range of [0.752, 0.8]. A histogram and CDF for the distribution on Mach number in cruise is shown in Fig. 4. Concurrent work on subproblem optimization in OpenMDAO will enable future work to more easily integrate constraints based on total time into design under uncertainty studies. This would enable the optimizer to choose an optimal trajectory based on overall mission time and not necessarily fix cruise Mach number.

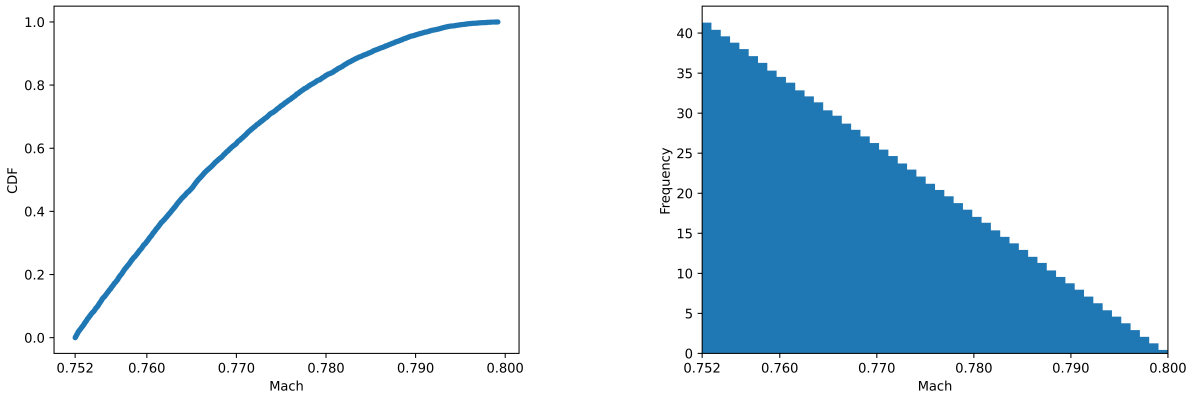

a) Cruise Mach CDF.

b) Cruise Mach histogram.

Fig. 4 Cruise Mach uncertain input distributions.

Uncertainty was also introduced into the problem by the amount of passenger specific payload weight (passengers plus their baggage) and expectations on how full the aircraft would be (load factor). A composite function was assembled that included uncertainty in passenger weight, passenger baggage weight, number of passenger bags, and aircraft load factor. For passenger weight, CDC data [26] were utilized to build a normal distribution for both expected weight of American men (μ = 199.8 lb, σ = 43.7 lb) and women (μ = 170.8 lb, σ = 46.5 lb). Weight distribution for children was more difficult to assess, so a uniform distribution between 20 lb and 180 lb was modeled. For a given load factor, the aircraft was assumed to be comprised of 49% women, 46% men, and 5% children [27]. With limited publicly available data for passenger luggage weight, it was assumed that carry-on luggage followed a normal distribution with $\mu = 20, \sigma$ = 5lbs and checked luggage followed a normal distribution of $\mu = 40s, \sigma$ = 10 lbs. In this case study 40% of passengers travelled with carry-on only, 55% checked one bag, and 5% checked two bags [28].

Average monthly load factor data from 1/1/2000 through 6/1/2024 published by the Federal Reserve [29] were used as the basis for the uncertain distribution for load factors. The years following September 11, 2001 (9/2001 - 9/2002) and the initial disruption to the airline industry from Covid-19 (3/2020 - 3/2021) were removed from the data set. As with the aircraft turnaround time, the load factor data available are averages which likely obscure some higher frequency data. Therefore, a Gaussian noise was added in an attempt to simulate some of the higher frequency data. Combining all the uncertainty derived from passenger weight, baggage, and load factors, the passenger specific component of payload was modeled with a normal distribution of μ = 30400 lb, σ = 5500 lb.

This research is focused on demonstrating the methodology while maintaining traceability to the source of the uncertainties and distributions within the problem. It is likely that an aircraft manufacturer or operator would have significant amounts of proprietary data that could replace distributions above. If an operator has historical data or projections on how their future fleet will be operated, designers could follow similar steps to tailor their designs to the actual or anticipated operations.

B. Baseline Uncertainty Analysis

Although the focus of this work is leveraging the previously developed analytical gradient capability for PCE in conceptual aircraft design, the integration of UQPCE with Aviary and OpenMDAO enables traditional coupled systems analysis and design space exploration with uncertainty. Prior to performing an optimization under uncertainty, a design space exploration incorporating uncertainty can provide insight into the uncertain space as a function of design variables. A high dimensional or unique uncertainty space can be difficult to visualize while potentially generating non-intuitive results.

Starting with the baseline N3CC model, uncertainty analysis was performed alongside parameter sweeps for wing span and sweep. Figure 5 shows four plots, each one with a constant sweep angle and varying span values. Note that the x-axis for span is the same for each figure as not all designs closed for all values of span across each of the sweep values. Gathering information on the fuel burn values from Fig. 5, the optimal design variable settings for span and sweep would be expected to occur between span = [135, 145] ft and sweep = [30, 40] deg, depending on the objective function formulation.

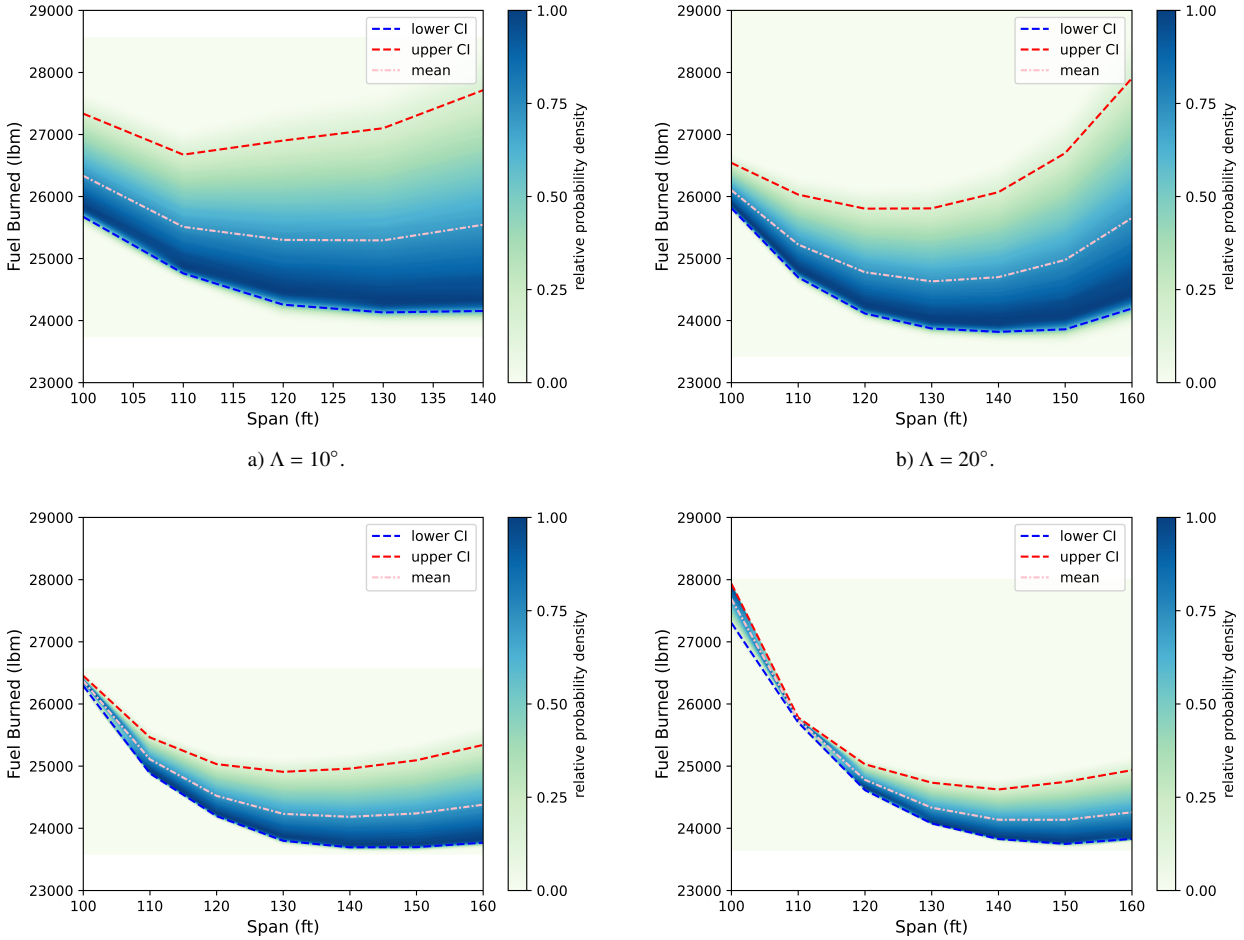

a) $\Lambda = 10°$.

b) $\Lambda = 20°$.

c) $\Lambda = 30°$.

d) $\Lambda = 40°$.

Fig. 5 Design space exploration with uncertainty for the base N3CC model.

C. Baseline Optimization

A deterministic optimization was performed for comparison to the optimization under uncertainty. The XDSM of this configuration is shown in Fig. 6 and the problem formulation is listed in Table 1. The N3CC model was optimized with the passenger payload set to the mean, 30,400 lb, and the nominal cruise Mach = 0.752 (equivalent total mission time = 430 min). The optimizer was allowed to manipulate wing span and sweep as well as the design gross mass to converge the design seeking to minimize fuel burn. Inside of the mission, wing span and sweep were connected to OpenVSP which was instantiated as an Aviary external subsystem. This enabled the recalculation of wing area, which was then connected to a custom wing mass calculation. This process was followed because core Aviary does not contain wing area calculations. A post-optimality uncertainty quantification was conducted using Aviary's off-design capability. A .JSON file containing the optimized aircraft configuration was exported. The UQPCE library was then used to sample within the uncertain cruise Mach number and passenger payload space. The resultant vehicle and mission outputs were then analyzed with Aviary Mission analysis using the fixed aircraft configuration. The resulting fuel burn information from the off-design missions was connected to UQPCE to generate estimates for uncertainty in fuel burn.

Table 1 Baseline Deterministic Problem Formulation

	Variable or Function	Size	Discipline
minimize	Fuel Burn	1	
with respect to	Wing Sweep	1	Aerodynamics
	Wing Span	1	
	Design Gross Mass	1	Weights
	Summary Gross Mass	1	
	Climb Duration	1	Trajectory
	Cruise Duration	1	
	Descent Duration	1	
	Mass	46	
	Distance	45	
subject to	Mass Residuals and Constraints	3	Weights
	Throttle Constraints	60	Propulsion
	Range Residual	1	Trajectory
	Pseudospectral Constraints	90	

D. Uncertainty Optimization

Integrating UQPCE into Aviary problems necessitated the development of a monolithic multi-mission optimization capability for Aviary, as described in Section II.C.1. Recall from Section II.B that to generate a PCE surrogate model, multiple samples from the uncertainty space are required. For this particular problem, the multiple samples within the uncertainty space lead to multiple vehicles with varying payload masses and cruise Mach values. Two uncertain optimizations were conducted with the same initial configuration. In both of the optimizations, the uncertain parameter information from Table 2 was initialized in UQPCE. UQPCE then generated samples from the uncertainty space resulting in multiple vehicles and missions which were then set in a monolithic multi-mission problem. The multi-mission problem is set up in a similar way as the baseline problem; however, fuel burn across all the missions is calculated simultaneously. Before being sent to the optimizer, the fuel burn values are vectorized for UQPCE to generate the PCE model. In the first of the two uncertain optimizations, the mean fuel burn was passed to the optimizer as the objective and the confidence interval on fuel burn was evaluated but not constrained. The XDSM of the first configuration is shown in Fig. 7 and the problem formulation is listed in Table 3. In this work, we adopt the convention of the † for input or outputs containing uncertain parameters in the XDSM. The design variables and their ranges are given in Table 4. In the second uncertain optimization, the upper bound on the 95% confidence interval (CI) of the fuel burn was the objective function, and otherwise the optimization remained unchanged. A fixed mission with three simple phases, climb, cruise, and descent, was simulated. The trajectory was fixed for each mission with the exception of some small design freedom given to the time to climb and descend, 15 minutes each. The flexibility given to climb time ensured that the heavier aircraft were still able to fly successfully. A full subproblem optimization capability, sometimes referred

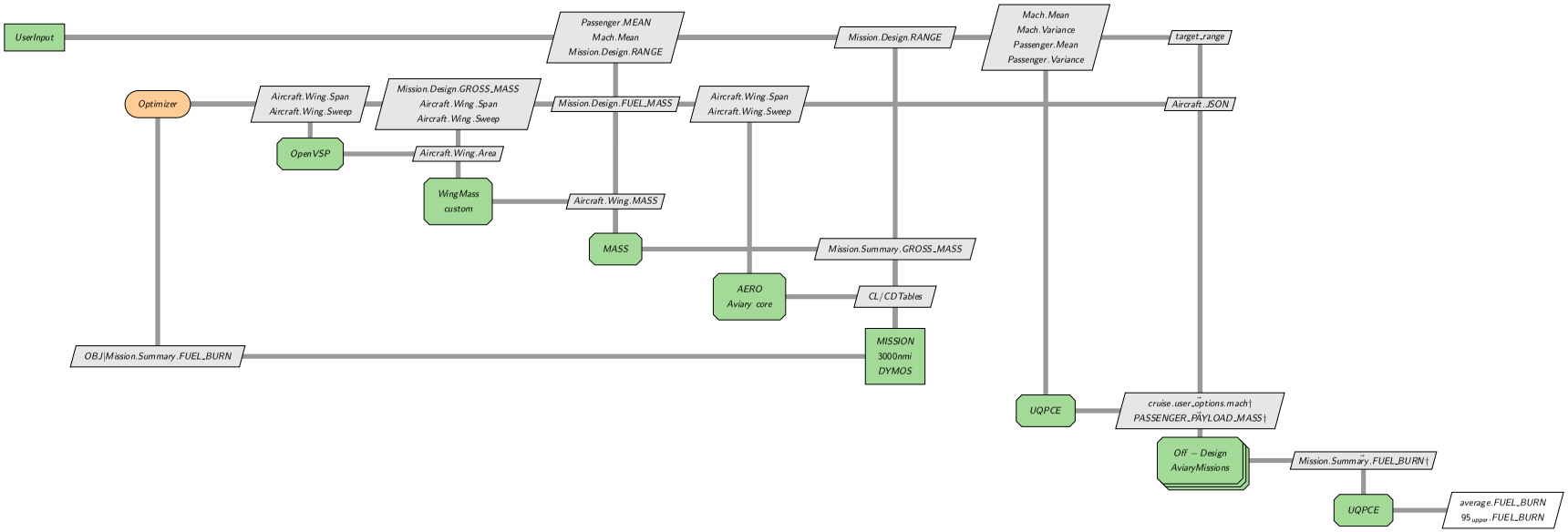

Fig. 6 Baseline optimization and post-optimality UQ.

to as nested optimization, would remove the need for the restrictions on trajectory as each individual mission could be optimized stand-alone within the larger problem.

Table 2 Uncertain parameters (aleatory)

Input	Distribution		
Cruise Mach	Triangular	Lower Bound: 0.752	Upper Bound: 0.80
Passenger Payload Weight, lb	Gaussian	$\mu = 30,450$	$\sigma = 5500$

Table 3 Optimization under uncertainty problem formulation

	Variable or Function	Size	Discipline
minimize	Mean or Upper Bound of the 95% CI Fuel Burn	1	
with respect to	Wing Sweep	1	Aerodynamics
	Wing Span	1	
	Design Gross Mass	1	Weights
	Summary Gross Mass	12	
	Climb Duration	12	Trajectory
	Cruise Duration	12	
	Descent Duration	12	
	Mass	552	
	Distance	540	
subject to	Mass Residuals and Constraints	36	Weights
	Throttle Constraints	720	Propulsion
	Range Residual	12	Trajectory
	Pseudospectral Constraints	1,080	

Table 4 Design variables

Input	Range
Takeoff Gross Weight (TOGW)	[80,000 , 200,000] lb
Λ	[10 , 45] deg
Span	[100 , 160] ft

E. Results and Discussion

This section will detail the results of the case study. Table 5 gives the results for the mean and confidence intervals of three optimization problems: a post-optimally uncertainty model from the deterministic case, the mean fuel burn optimization, and the upper bound of the 95% CI optimization. Although the deterministic design was already relatively robust, the mean optimization and the upper bound of the 95% CI optimization cases were able to produce trends as expected. Observing the mean value for each of the three cases, the mean optimization case produces the lowest mean value, whereas the CI-based optimization produced the largest. Likewise, the lowest upper bound for the 95% CI occurred when the optimizer was targeting that value in the CI optimization case.

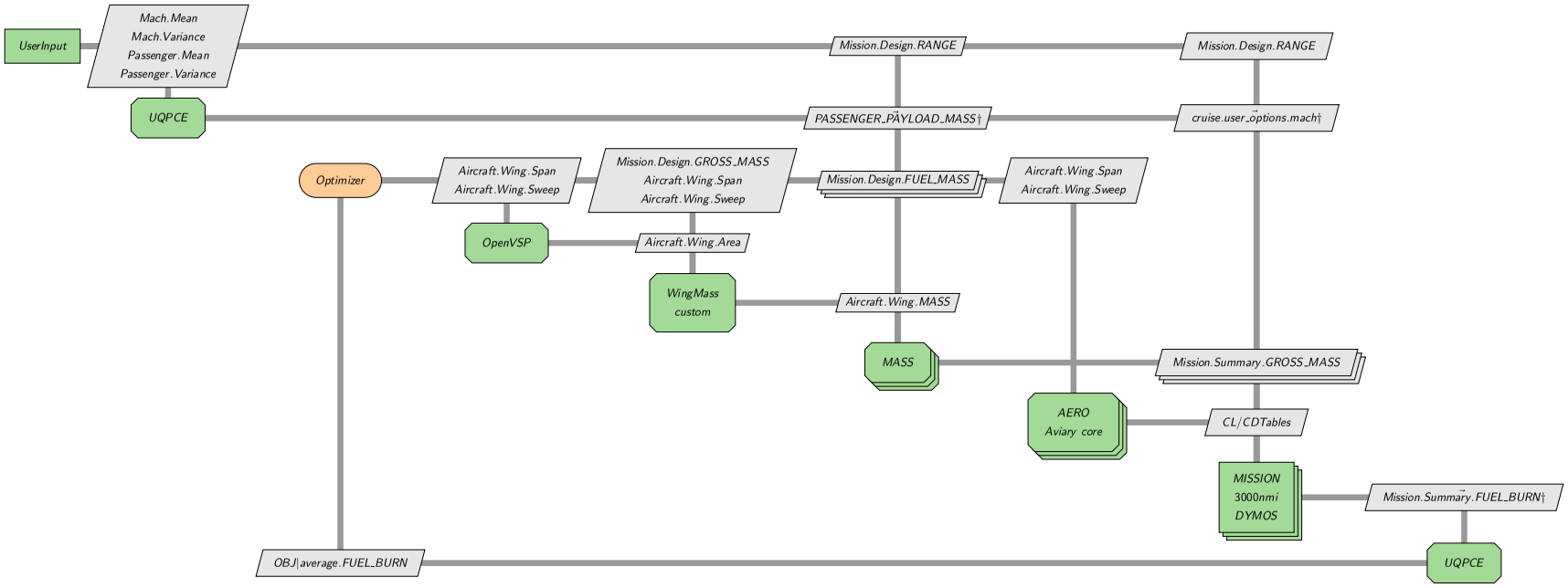

Fig. 7 Design under uncertainty.

Table 5 PCE model outputs

Objective	Mean	CI
Deterministic Fuel Burn	24,262	[23,370 , 25,302] lb
Mean Fuel Burn	24,201	[23,383, 25,332] lb
Upper Bound of the 95% CI Fuel Burn	24,404	[23,367, 25,046] lb

To better visualize the differences in the optimization results, the output fuel burn distributions for the three optimization problems are given in Fig. 8. To generate the output distributions for the deterministic problem, a post-optimality PCE model was built. The probability density functions (Fig. 8b) clearly show the lower shift in the mean with the mean optimization problem as outlined in Table 5. Additionally, the CI shift in the CI optimization problem is clearly seen in the cumulative distribution function (Fig. 8a). The optimizer in the CI case is trading a higher mean value for a lower upper bound on the 95% CI as evidence by the general shift of the CDF to the right, but a more abrupt tail than the other cases.

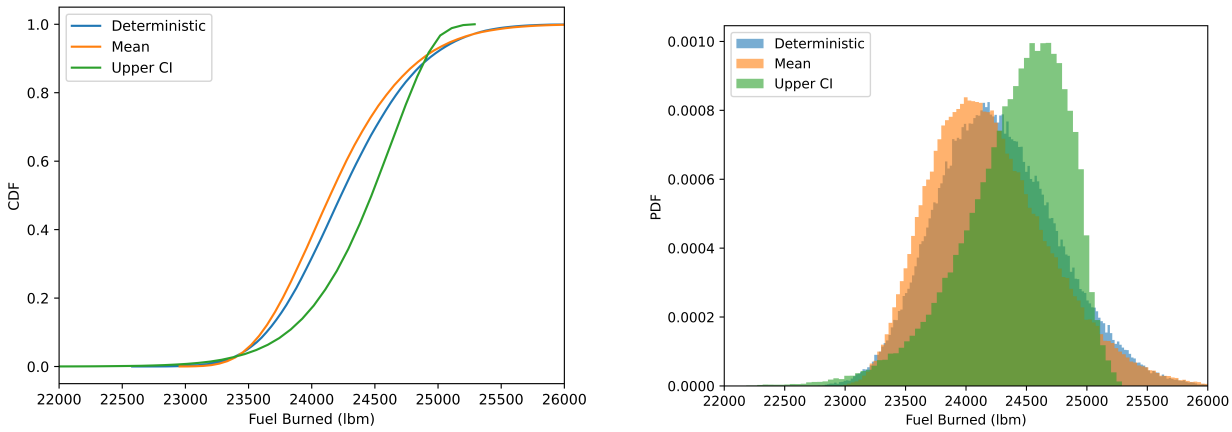

a) Comparison of CDFs from optimal designs.

b) Comparison of PDFs from optimal designs.

Fig. 8 Optimal design output distributions.

In Table 6 the design variables at their respective optimal conditions are shown for the three optimization problems. Operating Empty Weight (OEW) is shown instead of the design variable TOGW as it allows the designs to be compared equally without the variable passenger payload being considered. The designs considering uncertainty (mean fuel burn and upper bound of the 95% CI fuel burn) were both heavier than the deterministic case. As expected based on the first order relationship between wing sweep and wave drag, the sweep increased for the uncertain cases. If other structural or aeroelastic constraints (outside of the scope of this work) were imposed, the CI-optimized design would likely have been prevented from sweeping to the optimal design value of 39.1 deg, or extending span as far. The span for the 95% CI case was the longest, likely due to the increased passenger weight towards the tail of that respective distribution. For each of the three optimizations, the span was significantly longer than the baseline configuration. In addition to the lack of structural constraints, the core Aviary aerodynamics methodology overestimates the benefit of extending the span in comparison to higher fidelity methods such as VSPAero. However, given the integration of UQPCE, OpenMDAO, and Aviary, if a structural or aeroelastic model is already compatible with OpenMDAO, its constraints can be seamlessly integrated. As shown in Fig. 9, the increases in span and sweep are evident with the optimized geometries. In Table 7, the sensitivities at the optimal design conditions are given. As expected, given the two design variables, span and sweep, the sensitivity to uncertainty in Mach number decreases when the optimization problem is incorporating uncertainty. The sweep/Mach relationship is the only meaningful way the optimizer can reduce the overall uncertainty thus leading to higher sensitivity to passenger payload at the optimal design points. In comparing the computational costs for the deterministic case versus the uncertain optimizations, the uncertain optimizations took 13.6x more time to complete than

the deterministic one. Computational savings can be achieved through a more robust parallelization implementation of the processes for multi-mission optimization, which is left to future work.

Table 6 Optimal design variable values

Objective	Λ	Span	OEW
Deterministic Fuel Burn	34.0 deg	143.3 ft	80669 lb
Mean Fuel Burn	35.9 deg	141.6 ft	82318 lb
Upper Bound of the 95% CI Fuel Burn	39.1 deg	144.4 ft	83780 lb

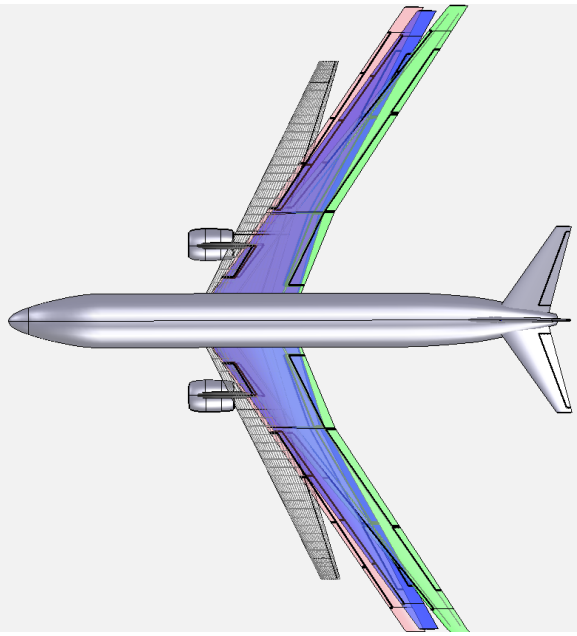

Fig. 9 N3CC optimized geometries. Gray (wireframe): initial, red: deterministic, blue: mean fuel burn, green: upper bound of the 95% CI.

Table 7 PCE model sensitivities

Objective	Mach	Passenger Payload
Deterministic Fuel Burn	41.5%	58.5%
Mean Fuel Burn	37.5%	62.5%
Upper Bound of the 95% CI Fuel Burn	24.4%	75.6%

F. Monolithic Optimization with Uncertainty in the Loop

The multi-mission optimization with uncertainty in the loop presented in Section III.D exposed some of the weaknesses of a monolithic multi-mission implementation coupled with uncertainty quantification. The first optimization with uncertainty was successful at minimizing fuel burn for the series of prescribed missions. Each individual aircraft and mission combination generated from the uncertainty space utilized a trajectory that minimized fuel burn, and these results added together created an overall fuel-burn optimal aircraft design. However, the introduction of an objective

related to the confidence interval in the second optimization with uncertainty caused unwanted behavior. Specifically, the optimizer attempted to fly some of the lighter passenger load missions in a sub-optimal way, consuming more fuel than expected. This allowed the optimizer to exploit the UQPCE model fit, decreasing its accuracy considerably as there were no constraints on the accuracy of the UQPCE fit. For this work, the solution identified was to restrict the trajectory enough that the optimizer could not select significantly non-optimal missions, but not restrict it enough such that the heavier payload missions could not close. This resulted in the problem formulation for the mission trajectory being fixed with the exception of 15 minutes of variability allowed in climb and decent time. This time value was generated based on a trial-and-error approach of analyzing cases throughout the uncertain space and observing optimizer behavior. The ability to perform nested subproblem optimization to ensure an optimal fuel burn for each mission within the uncertainty space will alleviate the need to add artificial time-based constraints and open up the design space to full coupled trajectory optimization.

IV. Summary

Multidisciplinary optimization for conceptual aircraft design under uncertainty with over 1100 variables and 1800 constraints has been demonstrated through the integration of the UQPCE libraries, OpenMDAO, and Aviary software libraries. Coupled trajectory, sizing, and aerodynamic optimization under uncertainty was performed. This work has demonstrated modeling a distribution outside of the usual academic distributions (normal, uniform, etc.) within the design under uncertainty problem. A more rigorous approach to identifying and characterising uncertainty parameters was taken. In the optimization under uncertainty problems in the case study, the optimizer was able to manipulate the uncertain space to produce more robust designs compared to the traditional deterministic design. The tools and methods developed for this work are modular in nature and adaptable to any gradient-based optimization for conceptual aircraft design. Future work will be dedicated to expanding the case study to include more disciplines, such as structural analysis, propulsion, acoustics, and cost modeling. Additionally, higher fidelity tools and methods will be incorporated in future work.

Acknowledgements

The work presented in this paper was performed with support from NASA's Transformational Tools and Technologies (TTT) and Advanced Air Transport Technology (AATT) Projects. Funding for those Projects is provided by NASA's Aeronautics Research Mission Directorate (ARMD). The authors would like to thank Kaushik Ponnapalli (NASA Glenn Research Center) for his assistance in setup and execution of the case study, Jatin Soni for his contributions to the multi-mission capability within Aviary, as well as the Aviary and OpenMDAO development teams.

References

[1] United States Federal Aviation Administration, "United States Aviation Climate Action Plan," , Nov. 2021. URL `https://www.faa.gov/sites/faa.gov/files/2021-11/Aviation_Climate_Action_Plan.pdf`.

[2] Phillips, B. D., Schmidt, J. N., Falck, R., and Aretskin-Hariton, E., "End-To-End Uncertainty Quantification with Analytical Derivatives for Design Under Uncertainty," *AIAA SCITECH 2024 Forum*, 2024. https://doi.org/10.2514/6.2024-0173.

[3] Welstead, J., and Felder, J. L., "Conceptual Design of a Single-Aisle Turboelectric Commercial Transport with Fuselage Boundary Layer Ingestion," *54th AIAA Aerospace Sciences Meeting*, 2016. https://doi.org/10.2514/6.2016-1027.

[4] Quinlan, J., Marien, T., Blaesser, N., Kirk, J., Perkins, H., and Fisher, K., "Far-Term Exploration of Advanced Single-Aisle Subsonic Transport Aircraft Concepts," *AIAA Aviation 2019 Forum*, 2019. https://doi.org/10.2514/6.2019-2880.

[5] Walker, E. L., Hemsch, M. J., and West IV, T. K., "Integrated Uncertainty Quantification for Risk and Resource Management: Building Confidence in Design," *53rd AIAA Aerospace Science Meeting*, 2015. https://doi.org/10.2514/6.2015-0501.

[6] Oberkampf, W. L., and Roy, C. J., *Verification and Validation in Scientific Computing*, Cambridge University Press, New York, NY, 2010.

[7] Phillips, B. D., and West IV, T. K., "Trim Flight Conditions for a Low-Boom Aircraft Under Uncertainty," *Journal of Aircraft*, Vol. 56, No. 1, 2019, pp. 53–67. https://doi.org/10.2514/1.C034932.

[8] Eldred, M. S., "Recent Advances in Non-Intrusive Polynomial Chaos and Stochastic Collocation Methods for Uncertainty Analysis and Design," *50th AIAA/ASME/ASCE/AHS/ASC Structures, Structural Dynamics, and Materials Conference*, 2009. https://doi.org/10.2514/6.2009-2274.

[9] Phillips, B. D., and Schmidt, J. N., "UQPCE v0.3.0," , 2023. Available at https://github.com/nasa/UQPCE.

[10] Phillips, B. D., Heath, C., and Schmidt, J. N., "System-Level Impact of Propulsive Uncertainties for Low-Boom Aircraft Concepts," *AIAA AVIATION 2020 Forum*, Virtual Event, 2020. https://doi.org/10.2514/6.2020-2730.

[11] Endo, M., and Phillips, B. D., "Uncertainty Quantification of CFD Model Assumptions Against Sonic Boom Noise Prediction of a Commercial Supersonic Transport," *AIAA SCITECH 2022 Forum*, 2022. https://doi.org/10.2514/6.2022-0401.

[12] Phillips, B. D., and West IV, T. K., "Aeroelastic Uncertainty Quantification of a Low-Boom Aircraft Configuration," *2018 AIAA Aerospace Sciences Meeting*, 2018. https://doi.org/10.2514/6.2018-0333.

[13] Eggert, C. A., White, L., Schmidt, J. N., Phillips, B. D., and Windous, Z. D., "Method for System-Level Multidisciplinary Uncertainty Analysis of Low-Boom Flight Vehicles," *AIAA SCITECH 2024 Forum*, 2024. https://doi.org/10.2514/6.2024-1876.

[14] Kirk, J., Frederick, Z. J., Guynn, M. D., Blaesser, N. J., Phillips, B. D., Fisher, K., Schneider, S. J., and Frederic, P., "Continued Exploration of the Electrified Aircraft Propulsion Design Space," *AIAA SCITECH 2023 Forum*, 2023. https://doi.org/10.2514/6.2023-1354.

[15] Fazal, B., Schmidt, J., Phillips, B. D., Ordaz, I., and Moore, K., "Integration of Uncertainty Quantification in a Model-Based Systems Analysis and Engineering Framework," *AIAA AVIATION FORUM AND ASCEND 2024*, 2024. https://doi.org/10.2514/6.2024-4559.

[16] Gray, J. S., Hwang, J. T., Martins, J. R. R. A., Moore, K. T., and Naylor, B. A., "OpenMDAO: An open-source framework for multidisciplinary design, analysis, and optimization," *Structural and Multidisciplinary Optimization*, Vol. 59, No. 4, 2019, pp. 1075–1104. https://doi.org/10.1007/s00158-019-02211-z.

[17] Bradbury, J., Frostig, R., Hawkins, P., Johnson, M. J., Leary, C., Maclaurin, D., Necula, G., Paszke, A., VanderPlas, J., Wanderman-Milne, S., and Zhan, Q., "JAX: composable transformations of Python+NumPy programs," , 2018. Available at http://github.com/google/jax.

[18] Aretskin-Hariton, E., Gratz, J., Kirk, J., Lyons, K., Jasa, J., Moore, K., Falck, R., Caldwell, D., Kuhnle, C., Recine, C., Hendricks, E., and Olson, E., "Multidisciplinary Optimization of a Transonic Truss-Braced Wing Aircraft using the Aviary Framework," *AIAA SCITECH 2024 Forum*, 2024. https://doi.org/10.2514/6.2024-1084.

[19] Gratz, J., Kirk, J., Recine, C., Jasa, J., Aretskin-Hariton, E., Moore, K., and Marfatia, K., "Aviary: An Open-Source Multidisciplinary Design, Analysis, and Optimization Tool for Modeling Aircraft With Analytic Gradients," *AIAA AVIATION FORUM AND ASCEND 2024*, 2024. https://doi.org/10.2514/6.2024-4219.

[20] Gratz, J., "Aviary," , 2024. Available at https://github.com/OpenMDAO/Aviary.

[21] Falck, R., Gray, J. S., Ponnapalli, K., and Wright, T., "dymos: A Python package for optimal control of multidisciplinary systems," *Journal of Open Source Software*, Vol. 6, No. 59, 2021, p. 2809. https://doi.org/10.21105/joss.02809.

[22] Galloway, T. L., and Waters, M. H., "Computer-Aided Parametric Analysis for General Aviation Aircraft," *SAE Paper 730332*, 1973.

[23] McCullers, L. A., "Aircraft Configuration Optimization Including Optimized Flight Profiles," *Recent Experiences in Multidisciplinary Analysis and Optimization*, 1984, pp. 395–412.

[24] Hahn, A., "Vehicle Sketch Pad: A Parametric Geometry Modeler for Conceptual Aircraft Design," *48th AIAA Aerospace Sciences Meeting Including the New Horizons Forum and Aerospace Exposition*, 2010. https://doi.org/10.2514/6.2010-657.

[25] OAG, "Formula One Science in Aircraft Turnarounds," , Apr. 2023. URL https://www.oag.com/blog/science-aircraft-turnarounds, accessed 11/15/2024.

[26] U.S. Department of Health and Human Services, "Anthropometric Reference Data for Children and Adults: United States 2015–2018," , Jan. 2021. URL https://www.cdc.gov/nchs/data/series/sr_03/sr03-046-508.pdf.

[27] Think With Google, "Digital trends: Air travelers July 2016," , Jul. 2016. URL https://www.thinkwithgoogle.com/consumer-insights/consumer-trends/digital-trends-air-travelers/, accessed 11/15/2024.

[28] Tripit, "So Long, Shoulder Season? New Survey Shows 85% of Americans Planning to Travel This Fall," , Sep. 2022. URL https://www.tripit.com/web/blog/news-culture/tripit-survey-shoulder-season-travel, accessed 11/15/2024.

[29] Federal Reserve Bank of St. Louis, "Load Factor for U.S. Air Carrier Domestic and International, Scheduled Passenger Flights," , Jul. 2024. URL https://fred.stlouisfed.org/series/LOADFACTOR, accessed 11/15/2024.